MATERIALS SCIENCE

Flexible biomimetic block copolymer composite for temperature and long-wave infrared sensing

Tae Hyun Kim[1], Zhun Zhou[1], Yeong Suk Choi[2]*, Vincenzo Costanza[1], Linghui Wang[1], Joong Hwan Bahng[1], Nicholas J. Higdon[1,3], Youngjun Yun[2], Hyunbum Kang[2], Sunghan Kim[2], Chiara Daraio[1]*

Biological compounds often provide clues to advance material designs. Replicating their molecular structure and functional motifs in artificial materials offers a blueprint for unprecedented functionalities. Here, we report a flexible biomimetic thermal sensing (BTS) polymer that is designed to emulate the ion transport dynamics of a plant cell wall component, pectin. Using a simple yet versatile synthetic procedure, we engineer the physicochemical properties of the polymer by inserting elastic fragments in a block copolymer architecture, making it flexible and stretchable. The thermal response of our flexible polymer outperforms current state-of-the-art temperature sensing materials, including vanadium oxide, by up to two orders of magnitude. Thermal sensors fabricated from these composites exhibit a sensitivity that exceeds 10 mK and operate stably between 15° and 55°C, even under repeated mechanical deformations. We demonstrate the use of our flexible BTS polymer in two-dimensional arrays for spatiotemporal temperature mapping and broadband infrared photodetection.

INTRODUCTION

Organic electronic materials are emerging as competitive alternatives to conventional silicon-based microelectronics because of their low-cost manufacturing (*1*, *2*) and multifunctionality (*3*, *4*). The ability to tailor their properties at the molecular level makes them appealing for a range of sensing applications, such as wearable and implantable devices, which require specific characteristics that are difficult to achieve with inorganic compounds, like flexibility and stretchability. The increasing demand for all-organic electronic devices has led to the developments of a growing number of soft and active materials for a variety of physical (*5*, *6*) and biochemical sensors (*7*, *8*), paralleled by the advancements in elastic substrates and conductors (*9*, *10*), as well as in their fabrication and integration strategies (*11*, *12*).

Organic thermal sensors have also been proposed for remote health care, robotics, and environmental and industrial monitoring applications (*10*, *13*). However, thermal sensing devices relying on organic materials are often limited by their response performance, which is not yet comparable to their inorganic counterparts. Several approaches have been suggested to improve materials' response to temperature, for example, by using inorganic fillers, nanocomposites, volume expansion, or the use of transistor-type devices for signal amplification (*14*–*17*). However, these strategies generally involve complex fabrication steps and device architectures, function in narrow temperature ranges, or provide limited response.

To overcome these limitations, it is necessary to develop organic materials that intrinsically present high thermal response and flexibility in a relatively simple scaffold that can be fabricated to scale with reproducible performance. However, the ability to design new materials depends on understanding the fundamental transport mechanism and structural dynamics in organic molecules (*18*, *19*) and on linking these properties to their functional characteristics. Although promising advances have been made, for example, with first principle simulations and data-driven approaches (*20*, *21*), the field is still lacking predictive models for the design and synthesis of such materials. One approach to design new materials is to gain insights from building blocks found in biological matters and to emulate their structures in synthetic materials.

Recent investigations of plant cell wall components reported that pectin, a structurally and functionally complex acid-rich polysaccharide (*22*), has a remarkable response to temperature (*23*–*25*). Pectin consists mostly of repeating units of D-galacturonic acid (Fig. 1A). At neutral pH, the D-galacturonic acid units of low-ester pectin form ionic bridges with Ca^{2+}, creating an "egg-box" complex in which cations are encapsulated (*26*, *27*). Increasing the temperature of a Ca^{2+}–cross-linked pectin results in an exponential increase in ionic conduction (*23*, *24*). However, pectin is most abundantly found in agricultural products, e.g., fruit peels, and its chemical composition is directly influenced by climate, plant origins, and extraction methods (*28*). Hence, devices fabricated with pectin, as a sensing element, present inconsistent electronic properties and demonstrate poor structural stability.

Here, we introduce a new flexible biomimetic thermal sensing (BTS) polymer that emulates the structure and functional motifs of pectin. The synthetic BTS polymer composite exhibits superior thermal sensitivity while also being mechanically robust and flexible (Fig. 1B). The basic architecture consists of an ABA-type triblock copolymer, synthesized through reversible addition-fragmentation chain transfer (RAFT) polymerization (fig. S1A), which is a versatile living radical polymerization method used to engineer structures with intrinsic mechanical flexibility (thermoplastic elastomers), suitable for organic electronic materials (*29*–*31*).

[1]Division of Engineering and Applied Science, California Institute of Technology, Pasadena, CA 91125, USA. [2]Samsung Advanced Institute of Technology (SAIT), Samsung Electronics, Suwon 16678, South Korea. [3]Division of Chemistry and Chemical Engineering, California Institute of Technology, Pasadena, CA 91125, USA.
*Corresponding author. Email: yeongsuk.choi@samsung.com (Y.S.C.); daraio@caltech.edu (C.D.)

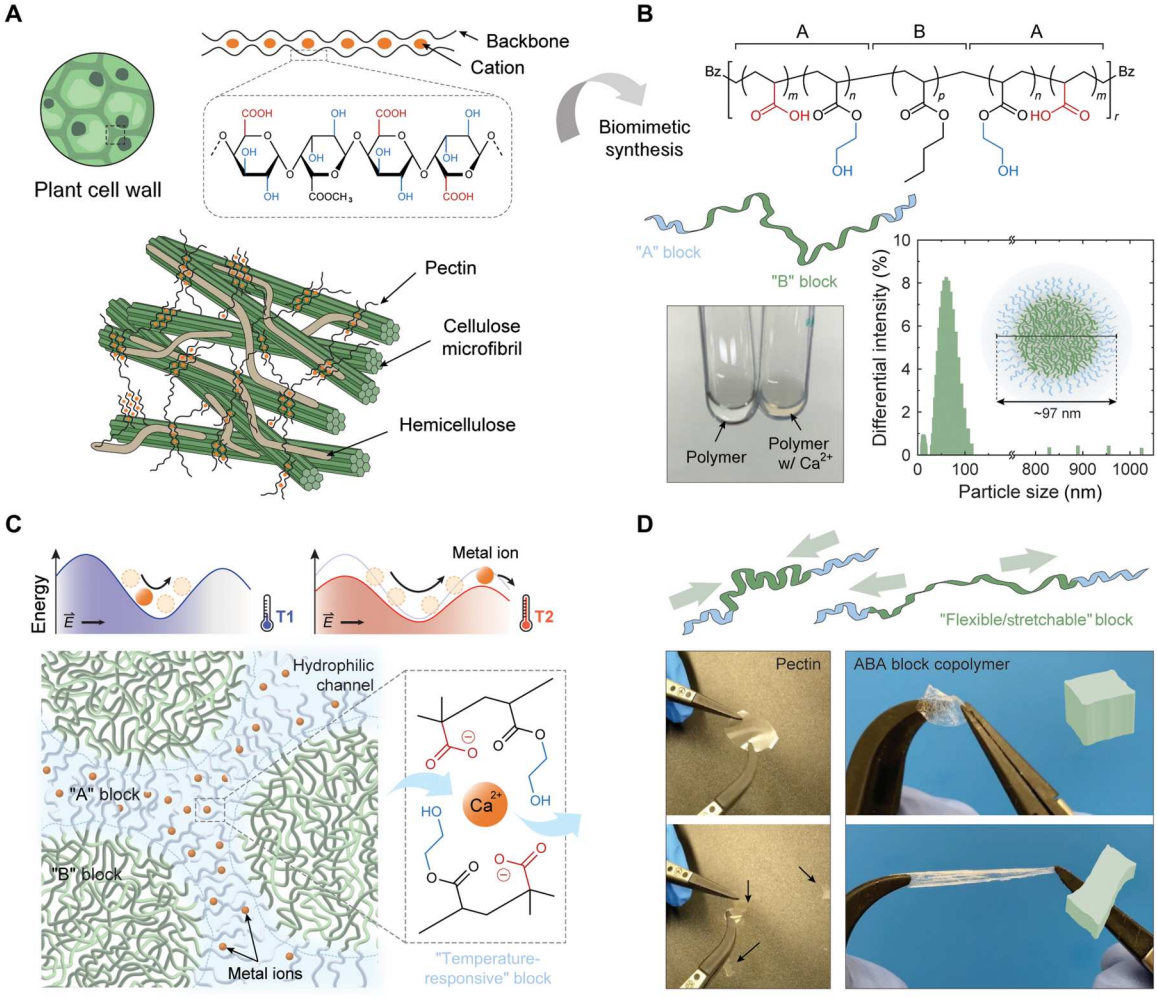

Fig. 1. Biomimetic design of the flexible BTS polymer. (**A**) Schematic illustration of the plant cell wall structure and of pectin. (**B**) Design of the ABA-type block copolymer, with $m = 5$, $n = 5$, $p = 100$, and $r = 85.7$. The hydrophilic A block, rich in carboxyl (red) and hydroxyl (blue) groups, is designed to electrostatically interact with metallic cations. The hydrophobic B block, composed of poly(*n*-butyl acrylate), is designed to provide mechanical flexibility and stretchability to the network. As shown in the particle size measurement (bottom right), the synthesized polymer exists in a colloidal state in ethanol due to phase separation. (**C**) Hypothesized mechanism governing the temperature response of the synthetic block copolymer. Rearrangement of the potential wells at low and high temperature in which the cations are confined (top). When an external electric field is applied, temperature rises cause an increase in ion migration through the hydrophilic channels formed between the colloidal particles in the polymer matrix (bottom). (**D**) Mechanical flexibility and stretchability of the synthetic block copolymer. The dried pectin film is prone to tear after a slight bending deformation (left), whereas the composite polymer is robust to repeated stretching motions because of the soft B block (right). The polymer is stretched 300% from its original shape.

RESULTS

Design of the flexible BTS polymer

To mimic pectin's temperature response, we conceptualize the polymer architecture by reducing the complex pectin structure to a simpler backbone, bearing only the minimally required cues for the desired functions. We hypothesize that the carboxyl groups, hydroxyl groups, and the conformation of sugar pockets are all essential components within the D-galacturonic acid that chelate divalent cations forming the egg-box complex (*26*, *32*). In the ABA architecture, the "A" blocks represent two flanking hydrophilic regions, displaying motifs that can bind with divalent cations, composed of random placement of 2-hydroxyethyl acrylate (HEA) and acrylic acid (AA). Upon chelating with divalent cations, the A blocks present a temperature response mechanism similar to that of pectin (Fig. 1C). However, the cationic interactions result in a "pseudo-cross-link," forming a hard segment with high glass transition temperature (T_g) (*33*). To add mechanical flexibility, the polymer is further modified by introducing low-T_g polymer molecules as soft segments. Poly(*n*-butyl acrylate), with low glass transition temperature ($T_g < -50$°C) (*34*), is inserted in the middle block "B," to serve as an elastic strand in the network and to make the polymer membrane stretchable (Fig. 1D). In ethanol, the synthesized polymer exists in colloidal states with an average particle diameter of 96.9 nm (Fig. 1B and fig. S1B). The hydrophilic-lipophilic balance value of the hydrophilic A block, calculated on the basis of Davies' method, is 13.03, corresponding to the oil-in-water emulsifier range (table S1).

To verify the functional roles of the polymer moiety relating to the temperature-dependent ion transport, we first characterize the structural components of the as-synthesized block copolymer, using gel permeation chromatography (GPC) and nuclear magnetic resonance (NMR) measurements (fig. S2). The synthesized polymer shows a weight-average molecular weight (M_w) of 113,600 g/mol with a dispersity of 1.08. This is similar to the M_w of natural pectin but with a much narrower weight distribution (*35*). The monomer feed ratio of the hydrophilic (hard) and hydrophobic (soft) segments is 1:5 (tables S2 and S3).

Adding divalent calcium ions into the flexible BTS polymer solution results in a cloudy appearance, revealing a network formation through ionic cross-links. The cross-linked solution is cast on a plastic sheet and dried to remove the remaining solvent (Fig. 2A). During this process, the mixture is monitored in situ using attenuated total reflectance–Fourier transform infrared (ATR-FTIR) spectroscopy to examine the film formation behavior. The characteristic peaks clearly elucidate structures of the designed polymer (Fig. 2B and table S4) and the presence of water contained inside (fig. S3). While the solvent evaporates, the neighboring chains of the block copolymer form interpolymer complexes (IPCs) between the AA-HEA functional groups. This interaction between the carbonyl oxygen and hydrogen of the hydroxyl group (hydrogen bonding) is suggested by the thermogravimetric analysis (TGA) profile (Fig. 2C) (*36*). Here, the IPCs may play a role in aggregating the colloidal particles to form ion transport channels between the interacting A blocks (Fig. 1C). At elevated temperatures, the number of ions overcoming the energy barrier increases, which leads to a higher diffusion constant and hopping rate between the coordination sites through the absorption of thermal energy and the polymer's segmental motion. Under an applied electric field, the probability of ions moving forward becomes favorable, generating a net current flow through the polymer network. The maximum amount of AA that can be involved in IPC formation is calculated as 86.13% (table S6).

To interrogate the importance of chemical composition within the A block, series of copolymers with varying ratio of AA to HEA are synthesized (Fig. 2D and table S7). The polymer film with even proportion of carboxyl-to-hydroxyl groups demonstrates the highest activation energy and temperature response. Modifying

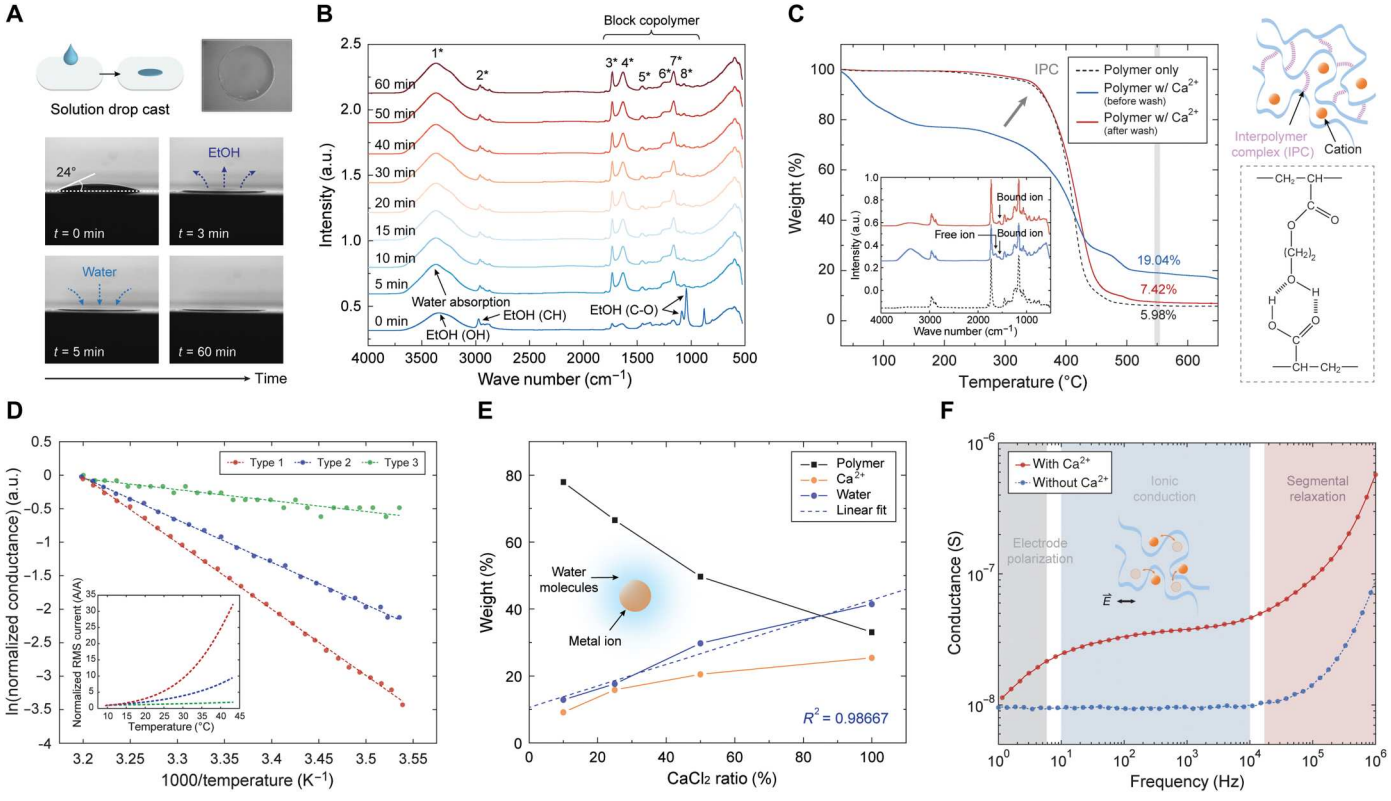

Fig. 2. Film formation behavior and component analysis of the block copolymer. (**A**) Digital images of the cross-linked block copolymer solution drop-casted on a flexible plastic substrate. The amount of cross-linking metal ions used for all tests is fixed to 100% unless otherwise stated. a.u., arbitrary units; EtOH, ethanol. (**B**) Time series of ATR-FTIR spectra after polymer deposition. During 1 hour of air dry, ethanol starts to evaporate, and subsequently, water is absorbed and saturated by the hygroscopic regions in the polymer matrix. *Peak assignments of the ATR-FTIR spectra (table S4). (**C**) TGA profile of the polymer film before and after washing in DI water. Titration analysis is performed to determine the percent of IPC formed in the composite film based on the amount of bounded metal ions after wash. Inset: Corresponding FTIR spectra of the films. (**D**) Arrhenius plot of different block copolymers. Activation energy compared between different polymer films with varying ratio of carboxyl to hydroxyl functional groups (type 1: $m = 5$, $n = 5$, $p = 100$; type 2: $m = 4$, $n = 7$, $p = 100$; type 3: $m = 10$, $n = 0$, $p = 100$). Inset: Corresponding thermal response of each type of polymer compared. Measurements are performed using the electrode design fabricated in fig. S6B with an AC voltage bias of 300 mV at 200 Hz. (**E**) Relation between the concentration of metal ions in the composite film and the amount of water adsorbed. Weight percentage of the polymer, Ca^{2+}, and water is calculated on the basis of the TGA profile and the coupled gas-phase FTIR spectra of the dried polymer films (fig. S5) with varying amount of $CaCl_2$ (table S5). A linear relationship is observed between the $CaCl_2$ concentration and water absorbed by the composite film. (**F**) Impedance spectra of the polymer film with and without Ca^{2+}.

this ratio to approximately 1:2 results in a >7-fold decrease in response, while films consisting of only the carboxyl groups lead to a response depletion. The result reveals that both hydroxyl and carboxyl groups collectively play important roles in chelation of Ca^{2+} and the subsequent formation of the egg-box–type interactions analogous to the coordination environment in pectin. Moreover, the high temperature response can be explained by the high-energy barrier created by strong binding forces between these side chains and calcium ions.

By varying the concentration of ions, the films are further profiled using TGA-FTIR to verify components from gas-phase diffusion (figs. S4 and S5). The linear relationship (R^2 = 0.987) between Ca^{2+} concentration and water in the film indicates that water absorption is mainly caused by metal ions (Fig. 2E). Last, to investigate the conducting species within the polymer matrix, electrochemical impedance spectroscopy analysis is performed. Polymer films with and without Ca^{2+} are prepared, and the system′s conductivity as a function of AC frequency is measured (Fig. 2F). The conductance profile of the film with no metal ions is flat until 10 kHz, whereas the one with Ca^{2+} shows an increase below 100 Hz due to electrode polarization followed by a plateau. This reveals that calcium cations are the major transporting charge carrier of the system.

Characterization of the flexible BTS polymer

To characterize the temperature response, we fabricate an array of circularly shaped interdigitated electrodes on a flexible plastic substrate and drop cast and dry 5 μl of the cross-linked BTS polymer solution on the electrodes′ surface (fig. S6, A and B). After mounting the samples on a custom-built thermal cycler, the output current is measured while applying an AC voltage of 300 mV at 200 Hz. The alternating signals enable stable measurements over time, reducing the possibility of ionic charge depletion caused by DC bias. Here, 300 mV is chosen on the basis of the minimum level of current (to avoid self-joule heating) that could be stably read from the sensor considering the signal noise floor at room temperature (RT).

The hydration state of organic materials closely correlates to the ionic transport and the material′s mechanical properties (*37*). To monitor the effect of water in the polymer′s performance, we dried the films under various conditions and repeat the measurements (Fig. 3A). When the polymer film is fully hydrated, a relatively low temperature response is observed. Under these conditions, conduction through water channels dominates the transport, suppressing the effect of ions, which is mainly responsible for the large temperature-dependent impedance changes. As the film is dried, removing unbound water from the chain, the response increases markedly, indicating the growing portion of Ca^{2+}-mediated transport (*25*). However, further dehydration results in a decreased response due to loss of conduction paths. A maximum root mean square (RMS) current response ($I_{45°C}/I_{15°C}$) of 80.04 A/A is exhibited over the defined temperature range. Such normalization approach has been adopted to compare between state-of-the-art thermal sensing materials, characterized under different measurement conditions. By measuring the output current at constant temperature in air, a sensing resolution of less than 8.68 mK is obtained with negligible hysteresis (fig. S6, C and D). Compared to the state-of-the-art thermal sensing materials, including vanadium oxide (*38*, *39*), inorganic devices (*40*–*42*), and natural pectin products (*23*, *24*), the overall temperature response of the resulting flexible BTS polymer composite is orders of magnitude higher (Fig. 3B).

To evaluate the materials′ response as a function of excitation frequency, we measure the samples′ impedance spectrum between 1 Hz and 5 MHz using 300 mV (Fig. 3C). At lower frequencies, in which the transport is mainly induced by ion migration, change of temperature results in a large variation of current. A maximum current response of over 160 A/A is evident around 20 Hz. At frequencies above the charge relaxation, transporting ions within the polymer are not able to follow the alternating electric field (polarization dominated) and no longer contribute to the temperature-dependent conduction behavior.

After conditioning the polymer film to its optimal hydration status, cyclic stability is evaluated by heating the sensor from 15° to 45°C for 6 hours while monitoring the current. Before measurements, a thin layer of parylene-C is conformally coated around the device to serve as a moisture barrier and electrical insulation. The device shows high stability (Fig. 3D and fig. S7) with minimum variation in current response, lying within the ±2.39% fluctuation boundary over 100 cycles of continuous use.

To characterize the effect of mechanical solicitations, the sensors are compressed or bent at different pressures and curvatures. Although a slight decrease in conduction is observed during compression (fig. S8), the average temperature error converted from the difference in current read-out, with and without loading, is less than 0.11°C up to a pressure of 250 kPa (Fig. 3E). This demonstrates that the sensor response is relatively insensitive to strain. Under bending deformations, an even lower temperature error is detected (Fig. 3F). To test whether the strain insensitivity persists after repetitive mechanical loading, we subject the samples to 100 cycles of bending (bending radius = 1.6 mm) or compression (to a maximum pressure of 25 kPa). The current remains similar to that of the as-fabricated samples, indicating high mechanical stability and elastic recovery. In contrast, dehydrated pectin films are brittle and prone to tear (Fig. 1D).

Spatiotemporal temperature mapping

We exemplify the applicability of our flexible BTS polymer composite for spatiotemporal temperature mapping and long-wave infrared (IR) photodetection. First, we create a flexible temperature sensing sheet, consisting of a 10 by 10 array of uniformly spaced sensors, placed 1 cm apart (Fig. 4A). We attach the sensor matrix on a circular glass plate with a point heat source located on its center and monitor the thermal gradient evolving across the glass surface in real time. The continuous heat flow along the plate′s radius is visualized in a time-dependent temperature map (Fig. 4B), obtained by measuring and interpolating the current variation on five polymer sensors. High temperature response, paired with its flexibility and compliance, offers opportunities in various engineering applications, such as batteries, packaging of perishable items, and wearable thermometers that require continuous spatial monitoring of temperature over three-dimensional surfaces.

Broadband long-wave IR sensing

Next, we experimentally demonstrate an uncooled, long-wave IR sensor that can detect thermal radiation across a wide spectral range (Fig. 5A). To reduce thermal loss via heat conduction, we fabricate electrodes on a thin polyimide (PI) membrane (2 μm) (fig. S9, A and B). To measure the responsivity ($\Delta I/P$), the entire device was placed in a hermetically sealed chamber with a zinc selenide (ZnSe) transmission window (fig. S9C). The sensor was biased at 1 V AC at

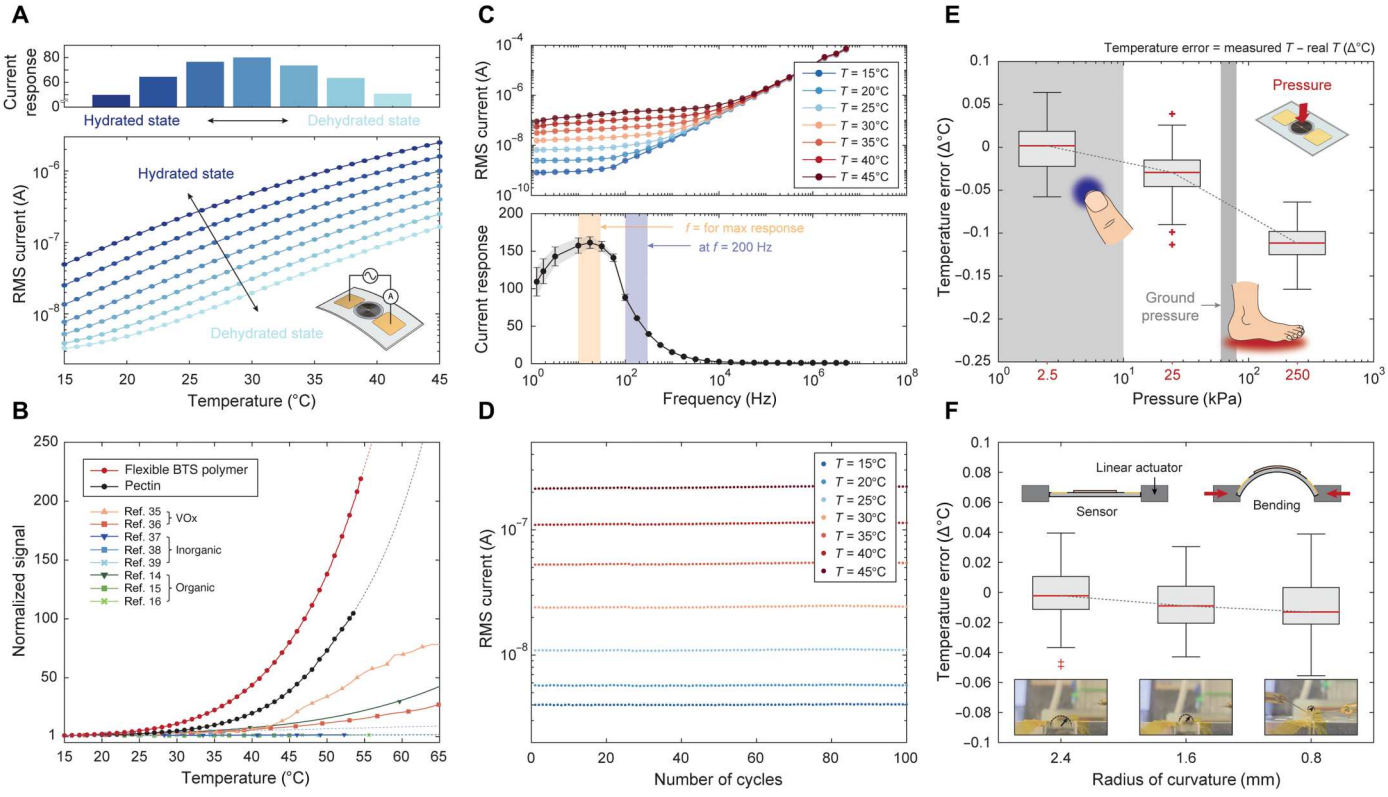

Fig. 3. Characterization of the flexible BTS polymer sensor. (**A**) Current variation as a function of temperature, measured between 15° and 45°C with an applied voltage of 300 mV at 200 Hz (bottom) and the corresponding current response calculated at different hydration levels (top). Darker blue lines represent higher hydration, and lighter blue lines represent lower hydration. Inset: Device schematic and configuration for electrical measurement. (**B**) Response comparison between state-of-the-art temperature sensing materials and devices, normalized with signals at 15°C. (**C**) Frequency-dependent current measured between 1 Hz and 5 MHz at varying temperatures (top) and the corresponding current response calculated when 300 mV was applied (bottom). Maximum response of 161.3 is obtained at 17.8 Hz. (**D**) Cyclic stability test over 100 cycles of continuous temperature oscillation between 15° and 45°C. (**E**) Temperature error extracted from the thermal sensor as a function of normal pressure and (**F**) bending strain (curvature). All plots represent data from polymer solution cross-linked with 100% concentration of $CaCl_2$.

200 Hz to increase the sensor's signal-to-noise ratio, ensuring no excessive self-heating caused by joule dissipation (fig. S10). Monitoring the current change as a function of applied power at 8.5-μm wavelength, we observe an exponential increase in current, following an Arrhenius behavior (Fig. 5B). To investigate the spectral responsivity of the sensor, we vary the wavelength of the incident IR with an applied power of 4 mW. The sensor responsivity is closely correlated to the spectral features of the polymer absorption spectrum, in which the characteristic peaks are located (8 to 14 μm) (Fig. 5C). Last, we use our sensor to detect IR-emitting objects near RT. With a hand waving motion above the sensor, a correlating current variation is detected (Fig. 5D). Current decrease is observed when the hand is covered with a sheet of paper. We repeat the measurement with an IR reflective aluminum sheet to verify whether this behavior is induced by thermal radiation. The aluminum layer blocks the irradiation emitted not only from the hand (movie S1) but also from the surrounding environment, resulting in a further decrease in sensor current.

DISCUSSION

The results presented here demonstrate a biomimetic approach to design a thermally responsive polymer for organic electronics. Inspired by the functional motifs in the pectin-Ca^{2+} complex, we create a block copolymer that demonstrates an extremely high thermal response with a sensing resolution of below 10 mK. By using a versatile synthetic procedure, we also show the ability to tailor physicochemical properties that enables optimization of the material's temperature sensitivity and endows mechanical flexibility and stretchability. Additional functionalities can be introduced by tailoring the polymer architecture and its side chains, for example, increasing its electrical conductivity, response time, or IR absorption spectrum for diverse thermal sensing platforms. The resulting material is stable under cyclic loading and insensitive to mechanical solicitations, extending its capability and potential use for wearable sensors and consumer electronics. In particular, these aspects have promise to affect technological advances in the medical or health care field that can allow continuous and noninvasive personalized monitoring of minute pathophysiological thermal stresses caused by disruption in homeostasis, infection, inflammatory responses, and mental stresses or sleep deprivation.

Although our BTS polymer has shown promising results, several challenges and room for improvements remain. Because of its nonlinear, exponential response to temperature and hydration-dependent sensitivity, a precalibration curve needs to be acquired before initial measurements, and care must be taken during sensor

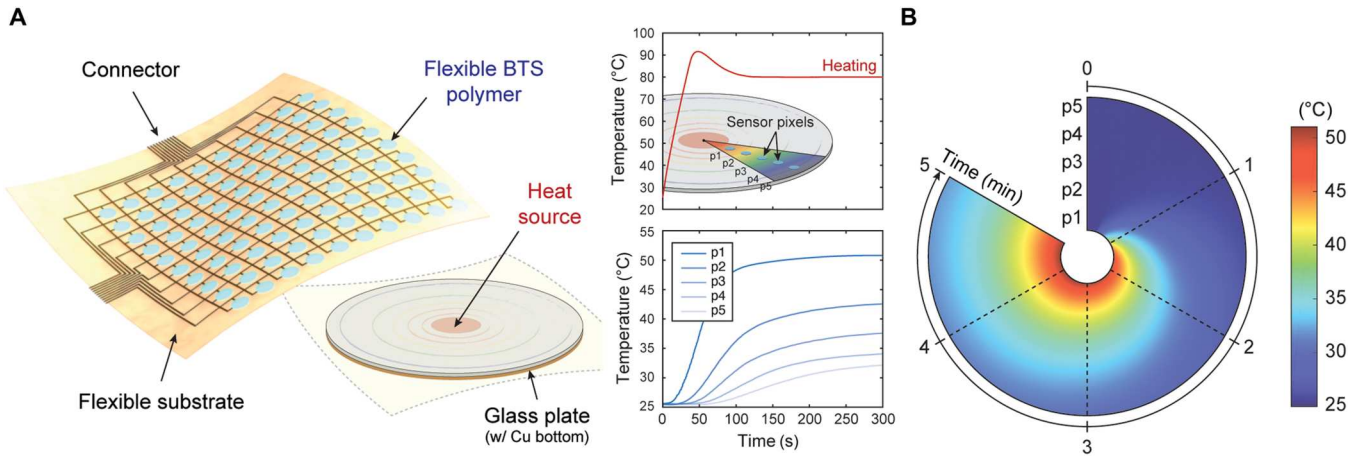

Fig. 4. Temperature sensing array based on flexible BTS polymer. (**A**) Schematic diagram of a flexible thermal sensor for large-area, multipixel temperature mapping. The sensor is placed on top of a glass plate where a heat source in the middle is used to generate a thermal gradient across the surface. Inset: Time versus temperature profile of the heat source (top) and the measured temperature value from each sensor (bottom). (**B**) Spatiotemporal reconstruction of the temperature evolution across the glass plate. Data are extracted from five sensor pixels along the radius of the glass slide.

packaging. In addition, an alternative synthesis procedure such as the continuous polymerization method will allow us to reduce batch-to-batch variation and enable mass production. Last, it will be of interest to further investigate the transport mechanism supplemented by molecular dynamic simulations to further delineate the thermal sensing behavior of the system to potentially improve the material sensitivity, dynamic range, or even the mechanical features by modifying the polymer composition and coordinating metal ions.

Interests on realizing all-organic electronic devices with functionalities that their inorganic counterparts cannot provide are on the rise. While many organic electronic components such as substrates, electrodes, and transistors have been developed, advancement and mechanistic understanding of the organic sensory elements have not progressed in parallel. To bridge this gap and to fully optimize the specific features of our flexible BTS polymer, further mechanistic studies accompanied by molecular dynamic simulations to delineate the exact origin of the high thermal response should be followed. We anticipate that our material and design concept can be used for fundamental studies of ion transport mechanisms in the form of such simplified polyelectrolytes, which can be generalized to different ionic conducting polymeric systems.

MATERIALS AND METHODS

Materials

HEA, *tert*-butyl acrylate (*t*-BA), *n*-butyl acrylate (*n*-BA) monomers, and a dual-functional chain transfer agent (CTA) *S*,*S*-dibenzyl trithiocarbonate (DBTTC) were purchased from Sigma-Aldrich. DBTTC was used to expedite the synthesis of the ABA polymer for multistep processing (*43*). Azobis (isobutyronitrile) (AIBN), a radical initiator, was purchased from Sigma-Aldrich and recrystallized from methanol before use.

Synthetic procedure of the ABA block copolymer

ABA-type block copolymers were prepared via RAFT polymerization (fig. S1A). During the entire polymer synthesis process, the resulting material was characterized using GPC and NMR (^{1}H NMR) (fig. S2) (*44*). First, N_2-purged HEA **1** (1.16 g, 10 mmol) and *t*-BA **2** (1.28 g, 10 mmol) were dissolved in 2 ml of dimethylformamide (DMF), followed by DBTTC **3** (29 mg, 0.1 mmol). The mixture was further purged with N_2 for 3 min. Next, AIBN (0.81 mg, 5 μmol) was added into the reactor and lastly stirred at 75°C under inert N_2 atmosphere. The reactor was cooled down and vented to air. The residual monomers (*t*-BA and HEA) were removed by vacuum, following precipitation in 100 ml of cold diethyl ether that resulted in a yellow oil of bis[p(*t*-BA_{10}-*r*-HEA_{10})] trithiocarbonate (macro-CTA). The yield of polymerization monitored using ^{1}H NMR was 80% (2.02 g). Next, the macro-CTA was mixed with N_2-purged *n*-BA **4** (12.8 g, 100 mmol) and AIBN (0.81 mg, 5 μmol), along with 15 ml of DMF. The mixture was purged again under N_2 for 3 min, followed by stirring at 75°C under N_2 atmosphere. The reactor was cooled down and vented to air. Residual *n*-BA was removed by vacuum to yield a protected form of ABA block copolymer, p[(*t*-BA_5-*r*-HEA_5)-*b*-(*n*-$BA)_{100}$-*b*-(*t*-BA_5-*r*-HEA_5)]$_r$. Here, a conversion rate of 81% was achieved (11.24 g). Last, 1 g of the protected polymer was dissolved in 3 ml of dichloromethane (DCM) and combined with 3 ml of trifluoroacetic acid (TFA). The deprotection reaction was carried out at RT and stirred overnight. DCM and TFA were removed by vacuum after precipitating the polymer in cold diethyl ether. As a result, a highly sticky yellow oil as the final form of the deprotected ABA block copolymer, p[(AA_5-*r*-HEA_5)-*b*-(*n*-$BA)_{100}$-*b*-(AA_5-*r*-HEA_5)]$_r$, was produced. The conversion of *tert*-butyl groups into AA was confirmed using ^{1}H NMR from the deprotected block copolymer (100% conversion to AA form).

Polymer characterization

The size of the colloidal particle formed in ethanol was measured using a zeta potential and particle size analyzer (Otsuka Electronics, ELSZ-2000) at RT (Fig 1B and fig. S1B). After dissolving the samples in deuterated DCM (CD_2Cl_2), NMR spectra were obtained using Bruker Ascend 500 (500 MHz). Spectral analysis was performed using Topspin 3.2 software. GPC was carried out in

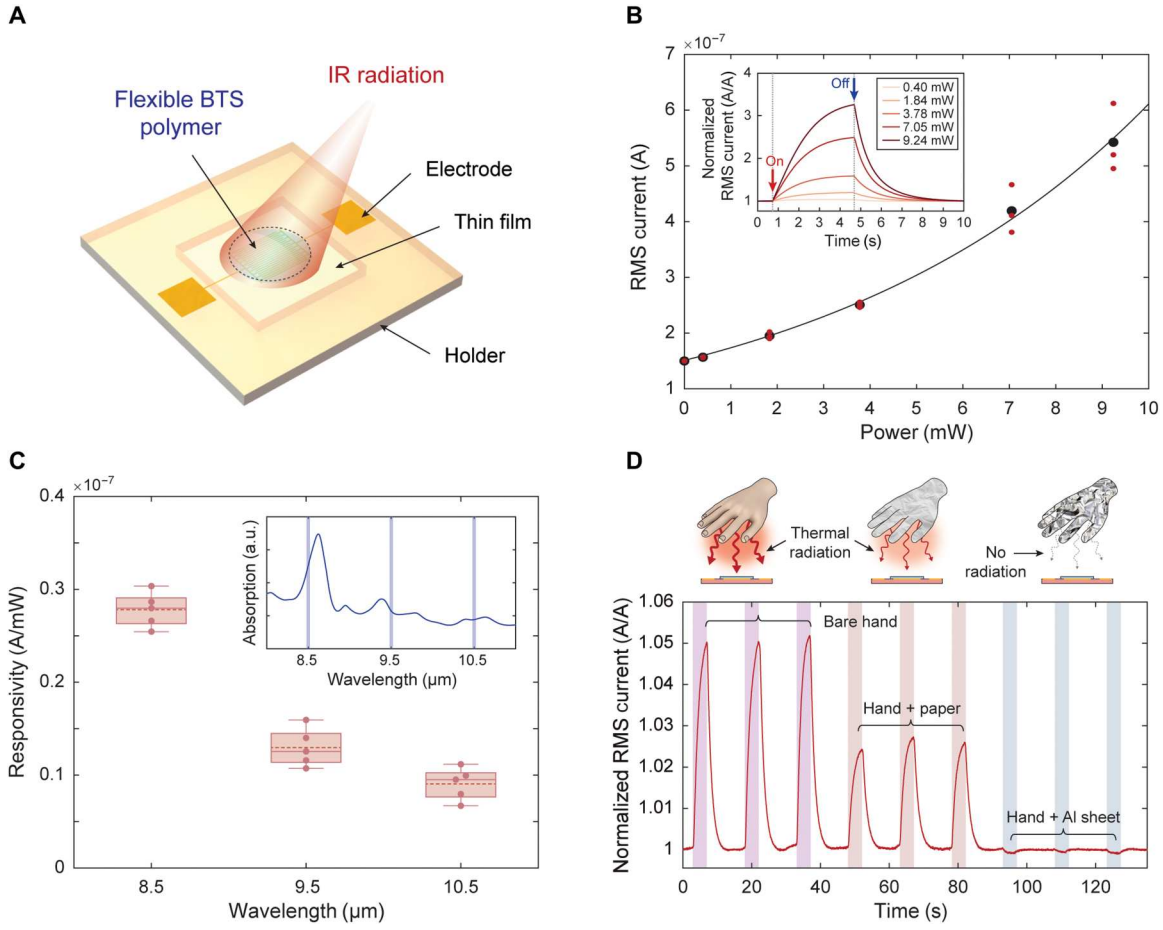

Fig. 5. IR sensor based on flexible BTS polymer. (**A**) Schematic of the fabricated long-wave, thermal IR detector. (**B**) Current as a function of IR power irradiated at a wavelength of 8.5 μm. Inset: Representative current profile during a 4-s period of IR exposure in air with different power. Current is measured using an applied voltage of 1 V at 200 Hz. (**C**) Responsivity of the IR detector at different wavelengths. Inset: Wavelength-dependent absorption intensity of the block copolymer. (**D**) Real-time detection of thermal radiation generated by a hand wave motion. Covering the hand with a sheet of paper, the rise in current is reduced due to limited transmission of irradiation power. Covering the hand with an aluminum sheet, no change or decrease in current is observed due to IR reflection.

tetrahydrofuran on two MZ-gel (10 μm) columns composed of styrene-divinylbenzene copolymer (Analysentechnik) connected in series with a miniDAWN TREOS multiangle laser light scattering detector. The film formation of the block copolymer was monitored in situ from the composite mixtures using ATR-FTIR spectroscopy using a Nicolet iS50 FTIR spectrometer. The synthesized block copolymer was dissolved in ethanol (1 mg/1 ml) with metal ions (0.3 M), mixed, placed on top of the ATR module, and continuously dried in air at 22°C under 23% relative humidity. The ATR-FTIR spectra were obtained as a function of time. Table S5 summarizes the composition of the tested mixtures.

TGA was carried out on dried composite films (20 mg) using a Discovery TGA (Thermo Fisher Scientific) with the following settings: ramp rate, 10°C/min; temperature range, 30° to 650°C; and N_2 flow rate, 10 ml/min. For material identification, TGA-FTIR measurements were performed in parallel to TGA to analyze the gas-phase FTIR spectra using a Nicolet iS50 FTIR spectrometer. The spectrometer was equipped with an auxiliary experiment module, composed of an optional mercury cadmium telluride detector, a 10-cm path-length nickel-plated aluminum flow cell, and an integrated digital temperature controller. After the integrated digital controller reached a constant 130°C temperature, FTIR spectra were collected every 5 min between 0 and 65 min. For each measurement, a total of 32 scans were averaged with 4 cm^{-1} resolution. Impedance spectroscopy analysis was performed using an impedance analyzer (Zurich Instruments MFIA). AC frequency was swept between 1 and 100 MHz (100 points) with a voltage biased at 1 V.

Percentage of IPC formed in the polymer film was calculated using the AA-Ca^{2+} titration method with the assumption that two AA functional groups are involved to form a coordination bond with a single Ca^{2+}. To begin with, the total amount of AA and metal ions (100% $CaCl_2$) in the polymer solution mixture was calculated (table S6). Next, the TGA and FTIR spectrum of the composite film was measured before and after washing with deionized (DI) water (Fig. 2C). To completely rinse out the unbound metal ions from the polymer matrix, the film was soaked in 200 cm^3 of DI water excessively with continuous stirring (120 rpm) at RT for 72 hours and dried. The proportion of Ca^{2+} bound to the polymer was calculated by subtracting the weight percentage between the two TGA profiles at 550°C, which corresponds to the residual content of metal ions (chelated Ca^{2+} with AA = 11.62%, free Ca^{2+} = 88.38%). The free and bound Ca^{2+} ions were recognized from the FTIR

spectra (inset of Fig. 2C) at 1640 and 1560 cm^{-1}, respectively. On the basis of the number of Ca^{2+} ions bound to the polymer film, the percentage of AA used to from IPCs was estimated as 86.13% (table S6).

Device fabrication

The block copolymer was dissolved in anhydrous ethanol at a concentration of 0.15 g/ml. Simultaneously, metal ion salt ($CaCl_2$) was dissolved in anhydrous ethanol at a concentration of 0.3 M. The ionically cross-linked polymer solution was obtained by mixing the two solutions at a volume ratio of 1:2. To fabricate the flexible temperature sensors, a thin sheet of polyester terephthalate (PET; 20 μm) was washed and attached to a 4-inch (100 mm) silicon wafer. On top, a layer of photoresist was spin-coated and patterned using the standard lithography process. The surface was then treated with O_2 plasma (Plasma-Therm SLR 720) followed by Ti/Au evaporation (CHA Mark 40 electron beam evaporator) with a thickness of 200/1000 Å. The entire sheet was immersed in acetone for metal lift-off, exposing the circularly shaped interdigitated electrodes (D = 4 mm, 30 μm wide with 20-μm spacing). Last, the PET sheet with the patterned electrodes was released, rinsed, and dried for use. Next, a total of 5 μl of cross-linked polymer solution was drop cast on top of each sensing pixel and dried at RT for 1 hour. To test different hydration status for optimal temperature response, the composite polymer was further dehydrated using dry air and sealed using a permeable PI tape. For cyclic studies, a thin layer of parylene-C (2 μm; ParaTech LabTop 3000 Parylene coater) was conformally coated around the devices to prevent water absorption or evaporation. External electrical connection was made using an anisotropic conductive film or an electrical probe set. The cross-sectional view of the fabrication process is shown in fig. S6A.

The IR bolometers were fabricated following similar steps but with slight modifications. An 8-inch (200 mm) glass wafer was cleaned in piranha solution for 30 min, rinsed using DI water, and dried under a nitrogen stream. The dried wafer was then plasma-treated. PI solution [10 weight % in dimethylacetamide (DMAc)] was spin-coated to a thickness of 2 μm and baked on a hot plate at 250°C for 60 min to cure the resin and fully remove the trapped DMAc in the film. Using a hard mask, a 100-nm-thick Au was thermally evaporated on the PI film to form the same interdigitated electrode design used above and rinsed using DI water, followed by a complete dry step. For handling purpose, a guiding layer of PI tape was placed on the wafer surface and cut into pieces with a knife. Last, each PI film containing a single electrode design was released and attached on a custom-made plastic holder with an opening at its center for air suspension (membrane structure). A total of 5 μl of cross-linked polymer solution was drop cast on top of the sensing pixel and dried at RT for 1 hour. Figure S9A illustrates the entire device fabrication process.

Experimental setup

A measurement stage was built to evaluate the temperature sensor (figs. S7A and S8A). The system was composed of a Peltier-Element (model Qc-31-1.4-8.5m) connected to a custom circuit board for controlled sample heating and cooling. The sensors were connected through electrical probes, and signals were measured using an impedance analyzer (Zurich Instruments MFIA). During measurements, the temperature of the Peltier block was continuously monitored with a Pt100 platinum resistance thermometer, which was calibrated by a FLIR thermal camera (model A655sc). For multiple cyclic tests, we generated a temperature sine wave between 15° and 45°C through the dedicated control board.

For IR measurement, the bolometer was placed in a hermetically sealed chamber (MPS-PT, Micro Probe System, Nextron Corp.) with a zinc selenide (ZnSe) transmission window (68-503, Edmund Optics). Figure S9C illustrates the optical setup. A quantum cascade laser (QCL; MIRcat-QT Mid-IR Laser) was used to apply IR radiation to the device at various wavelengths. The beam size of the QCL was 4.8 mm in diameter. The power of the emitted IR was calibrated using a power meter (PM16-401, Thorlabs) or an IR detector (PVMI-4TE, VIGO System). For both temperature and IR measurements, RMS current and phase from the impedance analyzer were continuously logged and visualized using a custom software (Python, LabVIEW).

Supplementary Materials

This PDF file includes:

Figs. S1 to S10
Tables S1 to S7
References

Other Supplementary Material for this manuscript includes the following:

Movie S1

REFERENCES AND NOTES

1. S. R. Forrest, The path to ubiquitous and low-cost organic electronic appliances on plastic. *Nature* **428**, 911–918 (2004).
2. A. N. Sokolov, M. E. Roberts, Z. Bao, Fabrication of low-cost electronic biosensors. *Mater. Today* **12**, 12–20 (2009).
3. H. Ling, S. Liu, Z. Zheng, F. Yan, Organic flexible electronics. *Small Methods* **2**, 1800070 (2018).
4. J. Kang, J. B.-H. Tok, Z. Bao, Self-healing soft electronics. *Nat. Electron.* **2**, 144–150 (2019).
5. B. C.-K. Tee, A. Chortos, A. Berndt, A. K. Nguyen, A. Tom, A. McGuire, Z. C. Lin, K. Tien, W.-G. Bae, H. Wang, P. Mei, H.-H. Chou, B. Cui, K. Deisseroth, T. N. Ng, Z. Bao, A skin-inspired organic digital mechanoreceptor. *Science* **350**, 313–316 (2015).
6. I. You, D. G. Mackanic, N. Matsuhisa, J. Kang, J. Kwon, L. Beker, J. Mun, W. Suh, T. Y. Kim, J. B.-H. Tok, Z. Bao, U. Jeong, Artificial multimodal receptors based on ion relaxation dynamics. *Science* **370**, 961–965 (2020).
7. N. Wang, A. Yang, Y. Fu, Y. Li, F. Yan, Functionalized organic thin film transistors for biosensing. *Accounts Chem. Res.* **52**, 277–287 (2019).
8. M. Y. Lee, H. R. Lee, C. H. Park, S. G. Han, J. H. Oh, Organic transistor-based chemical sensors for wearable bioelectronics. *Accounts Chem Res.* **51**, 2829–2838 (2018).
9. T. Sekitani, T. Someya, Stretchable, large-area organic electronics. *Adv. Mater.* **22**, 2228–2246 (2010).
10. J. Wang, M.-F. Lin, S. Park, P. S. Lee, Deformable conductors for human–machine interface. *Mater. Today* **21**, 508–526 (2018).
11. S. Wang, J. Xu, W. Wang, G.-J. N. Wang, R. Rastak, F. Molina-Lopez, J. W. Chung, S. Niu, V. R. Feig, J. Lopez, T. Lei, S.-K. Kwon, Y. Kim, A. M. Foudeh, A. Ehrlich, A. Gasperini, Y. Yun, B. Murmann, J. B.-H. Tok, Z. Bao, Skin electronics from scalable fabrication of an intrinsically stretchable transistor array. *Nature* **555**, 83–88 (2018).
12. H. Lim, H. S. Kim, R. Qazi, Y. Kwon, J. Jeong, W. Yeo, Advanced soft materials, sensor integrations, and applications of wearable flexible hybrid electronics in healthcare, energy, and environment. *Adv. Mater.* **32**, e1901924 (2020).
13. Y. H. Lee, O. Y. Kweon, H. Kim, J. H. Yoo, S. G. Han, J. H. Oh, Recent advances in organic sensors for health self-monitoring systems. *J. Mater. Chem. C* **6**, 8569–8612 (2018).
14. X. Ren, K. Pei, B. Peng, Z. Zhang, Z. Wang, X. Wang, P. K. L. Chan, A low-operating-power and flexible active-matrix organic-transistor temperature-sensor array. *Adv. Mater.* **28**, 4832–4838 (2016).
15. T. Q. Trung, S. Ramasundaram, B. Hwang, N. Lee, An all-elastomeric transparent and stretchable temperature sensor for body-attachable wearable electronics. *Adv. Mater.* **28**, 502–509 (2016).

16. Y. Yamamoto, S. Harada, D. Yamamoto, W. Honda, T. Arie, S. Akita, K. Takei, Printed multifunctional flexible device with an integrated motion sensor for health care monitoring. *Sci. Adv.* **2**, e1601473 (2016).
17. T. Yokota, Y. Inoue, Y. Terakawa, J. Reeder, M. Kaltenbrunner, T. Ware, K. Yang, K. Mabuchi, T. Murakawa, M. Sekino, W. Voit, T. Sekitani, T. Someya, Ultraflexible, large-area, physiological temperature sensors for multipoint measurements. *Proc. Natl. Acad. Sci. U.S.A.* **112**, 14533–14538 (2015).
18. H. Bronstein, C. B. Nielsen, B. C. Schroeder, I. McCulloch, The role of chemical design in the performance of organic semiconductors. *Nat. Rev. Chem.* **4**, 66–77 (2020).
19. M. Fahlman, S. Fabiano, V. Gueskine, D. Simon, M. Berggren, X. Crispin, Interfaces in organic electronics. *Nat. Rev. Mater.* **4**, 627–650 (2019).
20. S. Mogurampelly, O. Borodin, V. Ganesan, Computer simulations of ion transport in polymer electrolyte membranes. *Annu. Rev. Chem. Biomol.* **7**, 1–23 (2015).
21. P. Friederich, A. Fediai, S. Kaiser, M. Konrad, N. Jung, W. Wenzel, Toward design of novel materials for organic electronics. *Adv. Mater.* **31**, 1808256 (2019).
22. A. Peaucelle, S. Braybrook, H. Höfte, Cell wall mechanics and growth control in plants: The role of pectins revisited. *Front. Plant Sci.* **3**, 121 (2012).
23. R. D. Giacomo, C. Daraio, B. Maresca, Plant nanobionic materials with a giant temperature response mediated by pectin-Ca2^{+}. *Proc. Natl. Acad. Sci. U.S.A.* **112**, 4541–4545 (2015).
24. R. D. Giacomo, L. Bonanomi, V. Costanza, B. Maresca, C. Daraio, Biomimetic temperature-sensing layer for artificial skins. *Sci. Robot.* **2**, eaai9251 (2017).
25. V. Costanza, L. Bonanomi, G. Moscato, L. Wang, Y. S. Choi, C. Daraio, Effect of glycerol on the mechanical and temperature-sensing properties of pectin films. *Appl. Phys. Lett.* **115**, 193702 (2019).
26. G. T. Grant, E. R. Morris, D. A. Rees, P. J. C. Smith, D. Thom, Biological interactions between polysaccharides and divalent cations: The egg-box model. *FEBS Lett.* **32**, 195–198 (1973).
27. D. A. Powell, E. R. Morris, M. J. Gidley, D. A. Rees, Conformations and interactions of pectins .2. Influence of residue sequence on chain association in calcium pectate gels. *J. Mol. Biol.* **155**, 517–531 (1982).
28. B. R. Thakur, R. K. Singh, A. K. Handa, M. A. Rao, Chemistry and uses of pectin—A review. *Crit. Rev. Food Sci.* **37**, 47–73 (1997).
29. K. Matyjaszewski, J. Xia, Atom transfer radical polymerization. *Chem. Rev.* **101**, 2921–2990 (2001).
30. S. Yamago, Precision polymer synthesis by degenerative transfer controlled/living radical polymerization using organotellurium, organostibine, and organobismuthine chain-transfer agents. *Chem. Rev.* **109**, 5051–5068 (2009).
31. G. Moad, E. Rizzardo, S. H. Thang, *Toward Living Radical Polymerization* (2008), vol. 41 of *Accounts of Chemical Research*.
32. L. Cao, W. Lu, A. Mata, K. Nishinari, Y. Fang, Egg-box model-based gelation of alginate and pectin: A review. *Carbohyd. Polym.* **242**, 116389 (2020).
33. J. Furukawa, A theory of pseudo cross-link. *Polym. Bull.* **7**, 23–30 (1982).
34. E. A. DiMarzio, J. H. Gibbs, Glass temperature of copolymers. *J. Polym. Sci.* **40**, 121–131 (1959).
35. M. Y. Sayah, R. Chabir, H. Benyahia, Y. R. Kandri, F. O. Chahdi, H. Touzani, F. Errachidi, Yield, esterification degree and molecular weight evaluation of pectins isolated from orange and grapefruit peels under different conditions. *PLOS ONE* **11**, e0161751 (2016).
36. G. A. Mun, V. V. Khutoryanskiy, G. T. Akhmetkalieva, S. N. Shmakov, A. V. Dubolazov, Z. S. Nurkeeva, K. Park, Interpolymer complexes of poly(acrylic acid) with poly(2-hydroxyethyl acrylate) in aqueous solutions. *Colloid Polym. Sci.* **283**, 174–181 (2004).
37. J. W. H. Schymkowitz, F. Rousseau, I. C. Martins, J. Ferkinghoff-Borg, F. Stricher, L. Serrano, Prediction of water and metal binding sites and their affinities by using the Fold-X force field. *Proc. Natl. Acad. Sci. U.S.A.* **102**, 10147–10152 (2005).
38. B. Wang, J. Lai, H. Li, H. Hu, S. Chen, Nanostructured vanadium oxide thin film with high TCR at room temperature for microbolometer. *Infrared Phys. Techn.* **57**, 8–13 (2013).
39. J. Dai, X. Wang, S. He, Y. Huang, X. Yi, Low temperature fabrication of VOx thin films for uncooled IR detectors by direct current reactive magnetron sputtering method. *Infrared Phys. Techn.* **51**, 287–291 (2008).
40. J. Kim, M. Lee, H. J. Shim, R. Ghaffari, H. R. Cho, D. Son, Y. H. Jung, M. Soh, C. Choi, S. Jung, K. Chu, D. Jeon, S.-T. Lee, J. H. Kim, S. H. Choi, T. Hyeon, D.-H. Kim, Stretchable silicon nanoribbon electronics for skin prosthesis. *Nat. Commun.* **5**, 5747 (2014).
41. J. Park, M. Kim, Y. Lee, H. S. Lee, H. Ko, Fingertip skin–inspired microstructured ferroelectric skins discriminate static/dynamic pressure and temperature stimuli. *Sci. Adv.* **1**, e1500661 (2015).
42. R. C. Webb, A. P. Bonifas, A. Behnaz, Y. Zhang, K. J. Yu, H. Cheng, M. Shi, Z. Bian, Z. Liu, Y.-S. Kim, W.-H. Yeo, J. S. Park, J. Song, Y. Li, Y. Huang, A. M. Gorbach, J. A. Rogers, Ultrathin conformal devices for precise and continuous thermal characterization of human skin. *Nat. Mater.* **12**, 938–944 (2013).
43. H. U. Kang, Y. C. Yu, S. J. Shin, J. H. Youk, One-step synthesis of block copolymers using a hydroxyl-functionalized trithiocarbonate RAFT agent as a dual initiator for RAFT polymerization and ROP. *J. Polym. Sci. Part Polym. Chem.* **51**, 774–779 (2013).
44. D. G. Hawthorne, G. Moad, E. Rizzardo, S. H. Thang, Living radical polymerization with reversible addition–fragmentation chain transfer (RAFT): Direct ESR observation of intermediate radicals. *Macromolecules* **32**, 5457–5459 (1999).
45. W. Wang, Q. Zhang, Synthesis of block copolymer poly (n-butyl acrylate)-b-polystyrene by DPE seeded emulsion polymerization with monodisperse latex particles and morphology of self-assembly film surface. *J. Colloid Interf. Sci.* **374**, 54–60 (2012).
46. A. M. Kubo, L. F. Gorup, L. S. Amaral, E. Rodrigues-Filho, E. R. de Camargo, Heterogeneous microtubules of self-assembled silver and gold nanoparticles using alive biotemplates. *Mater. Res.* **21**, e20170947 (2018).
47. E. Vargün, A. Usanmaz, Polymerization of 2-hydroxyethyl acrylate in bulk and solution by chemical initiator and by ATRP method. *J. Polym. Sci. Part Polym. Chem.* **43**, 3957–3965 (2005).
48. D. Tang, B. A. J. Noordover, R. J. Sablong, C. E. Koning, Metal-free synthesis of novel bio-based dihydroxyl-terminated aliphatic polyesters as building blocks for thermoplastic polyurethanes. *J. Polym. Sci. Part Polym. Chem.* **49**, 2959–2968 (2011).

Acknowledgments: We acknowledge the critical support and infrastructure provided for this work by The Kavli Nanoscience Institute at Caltech. We would like to thank C. Heo and the Process Technology Group at SAIT for technical support during IR device fabrication; S. Han, M. S. Jang, and B. Min at the Korea Advanced Institute of Science and Technology (KAIST) for advice on the IR measurements; and H. B. Moon, Y. H. Jang, and N. Kim at Nextron Corp. for use of the Micro Probe System. **Funding:** This work was supported by the Samsung Electronics SAIT, GRO Program (C.D.), and by the Schwartz/Reisman Collaborative Science Program (C.D.).
Author contributions: T.H.K., Z.Z., V.C., L.W., and C.D. conceived the idea and designed the research. Z.Z., Y.S.C., and J.H.B. synthesized the block copolymer. T.H.K., Z.Z., Y.S.C., and S.K. performed the particle size analysis, NMR, GPC, ATR-FTIR, TGA-FTIR, and the titration experiments for material characterization and analyzed the data. N.J.H. provided technical support during the FTIR analysis. T.H.K. designed and fabricated the temperature sensor. T.H.K., V.C., and L.W. built the custom measurement stage for thermal characterization, conducted electrical measurements, carried out mechanical tests on the block copolymer, and analyzed the data. T.H.K., Y.S.C., Y.Y., and H.K. designed and fabricated the IR detector. T.H.K. performed the IR measurements and analyzed the data. C.D. supervised the project. T.H.K., Y.S.C., and C.D. cowrote the manuscript. All authors commented on the manuscript. **Competing interests:** T.H.K., Z.Z., Y.S.C., V.C., L.W., and C.D. are the named inventors on the patent assigned to Samsung Electronics Co Ltd. and the California Institute of Technology regarding the biomimetic block copolymer and its application for temperature and IR sensing. Application number: US20220056188A1 (2022-02-24). Status: Pending. T.H.K., Z.Z., Y.S.C., V.C., L.W., and C.D. are the named inventors on the issued patent number US11492420B2, granted to Samsung Electronics Co. Ltd. and the California Institute of Technology regarding composites and IR absorbers (2022-11-08). Status: Active. V.C., C.D., and Z.Z. are the named inventors on the patent assigned to the California Institute of Technology regarding the ABA-type block copolymers for temperature sensing and flow meters. Application number: US20200353729A1 (2020-11-12). Status: Pending. V.C. and C.D. are the named inventors on the issued patent number US10345153B2, granted to the California Institute of Technology regarding gel-based thermal sensors (2019-07-09). Status: Active. C.D. is currently affiliated with Meta Reality Labs. The other authors declare that they have no competing interests. **Data and materials availability:** All data needed to evaluate the conclusions in the paper are present in the paper and/or the Supplementary Materials.

Submitted 22 July 2022
Accepted 9 January 2023
Published 10 February 2023
10.1126/sciadv.ade0423